Synthesis of optically active chiral mesoporous molybdenum carbide film

Fusheng Zhang, Xintong Zheng, Cunli Wang, Dongdong Wang,
Xingya Xue, Guangyan Qing

PII: S1226-086X(20)30532-3

DOI: https://doi.org/10.1016/j.jiec.2020.11.023

Reference: JIEC 5304

To appear in: *Journal of Industrial and Engineering Chemistry*

Received Date: 30 September 2020

Revised Date: 25 November 2020

Accepted Date: 25 November 2020

Please cite this article as: Zhang F, Zheng X, Wang C, Wang D, Xue X, Qing G, Synthesis of optically active chiral mesoporous molybdenum carbide film, *Journal of Industrial and Engineering Chemistry* (2020), doi: https://doi.org/10.1016/j.jiec.2020.11.023

Synthesis of optically active chiral mesoporous molybdenum carbide film

Fusheng Zhang,[a,b] Xintong Zheng,[a,c] Cunli Wang,[a] Dongdong Wang,[a] Xingya Xue,[a] Guangyan Qing[a,d]*

[a] Key Laboratory of Separation Science for Analytical Chemistry, Dalian Institute of Chemical Physics, Chinese Academy of Sciences, Dalian, Liaoning, 116023, P. R. China

[b] University of Chinese Academy of Sciences, Beijing, 100049, P. R. China

[c] Pharmacy College, Dalian Medical University, Dalian, Liaoning, 116044, P. R. China

[d] Key Laboratory of Advanced Energy Materials Chemistry (Ministry of Education), College of Chemistry, Nankai University, Tianjin, 300071, P. R. China

Graphical abstract

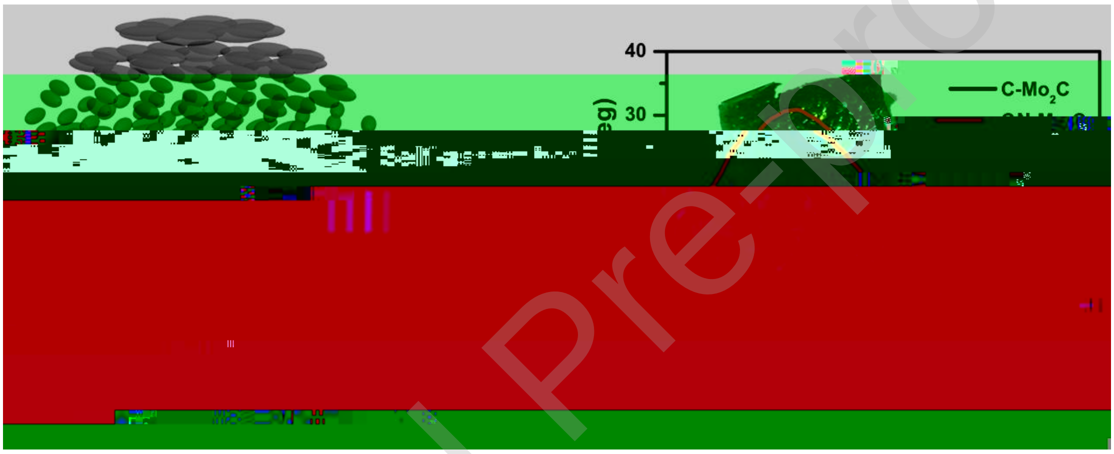

Abstract

A chiral nematic mesoporous molybdenum carbide film (CN-Mo_2C) was fabricated through the self-assembly of cellulose nanocrystal with peroxomolybdate. CN-Mo_2C exhibits a tunable chiral nematic structure by varying the ratio of constituents, enabling a surface area of 210 m^2 g$^{\ 1}$. Importantly, it shows a typical chiroptical feature through polarized optical microscopy and circular dichroism spectral analysis. As it has an excellent conductivity of $2.4 \times 10^{\ 2}$ S cm$^{\ 1}$, we try to use CN-Mo_2C in the electrocatalytic HER production, presenting an efficient H_2 production capacity. It is a

versatile synthetic strategy that can conveniently enable other large-area macroscopic chiral metal-based materials.

Keyword: Chirality; Cellulose nanocrystal; Molybdenum; Structural tuning; Chiroptical property

Introduction

Chiral inorganic materials have attracted much attention because of their novel properties and wide applications in chiral plasmonics[1], chiroptical sensing[2], and asymmetric catalysis[3]. It is motivated by the self-evident significance of chirality for physics, chemistry, and biomedicine[4, 5]. Meanwhile, inorganic nanocrystals can be easily modulated through altering their size, shape, and ingredient, which is a promising platform for understanding the chiral origins. Research in this area points out the chiroptical activity can 024 5.67 Tm Tm[(-)] TJET EM--57(n)-9(a)4(noc)4(r)-16(y 0 0 1 90.024 406.8D to-prepare chiral inorganic film can have wide application prospects due to their operability in the application process.

Cellulose nanocrystal (CNC) is obtained by sulfuric acid-catalyzed hydrolysis of biomass and then hierarchically self-organize into the chiral nematic phase through electrostatic repulsion among sulfates[14]. A pioneer MacLachlan has reported many modes of co-assemble CNC with multiple precursors in aqueous solution to fabricate chiral nematic iridescent films. Because of the surface sulfate esters on CNCs, it is sensitive to the ionic strength. Varying the ionic strength in the assembly process is a powerful approach for controlling the reflected color of the iridescent film.[15] Color tuning is also possible for the pH values or precursor loading.[16] CNC as a bio-template can make the chiral nematic structure deliver into silica[17], carbon[18], titanium dioxide [19], cupric oxide[20], cobalt ferrite[21], and other metal-based matrixs[22, 23]. The pores of these long-range hierarchical materials are aligned in directional layers through a rotating stack. Thereupon, CNC-derived chiral nematic inorganic materials have been currently used for the development of novel sensors, catalyst supports, and energy storage8] optimization, the satisfactory resulting made the PM possible to retain the chiral nematic phase for the construction of Mo-based freestanding chiral nanostructured materials[27, 28]. Furthermore, this strategy can be realized in other peroxometallate compounds to fabricate chiral nematic inorganic nanostructure, including peroxotitanate, peroxovanadate, and peroxozirconate. As proof of concept, the incorporation of the PM solution into the CNC suspension fabricated a colorful PM/CNC composite film with the chiral nematic organization for the first time. Subsequent carbonization of the composite film and magnesiothermic reduction, a freestanding chiral nematic mesoporous molybdenum carbide film (CN-

Experimental section

Materials and Characterization. All reagents and solvents without further purification including molybdenum powder (99.5%), ammonium molybdate (99%), molybdenum carbide (99.9%), hydrogen peroxide (H_2O_2, 30%) through standard

Thermogravimetric analysis (TGA) was measured using a Diamond TG/DTA Instrument (STA 449 F3, Netzsch, Germany) up to 800°C with a heating rate of 10.0°C min ^{1}. Electrical conductivity was measured by using the standard four-probe method with at least three measurements.

Preparation of PM/CNC composite film (MCF). Molybdenum powder (5 g) was slowly added into H_2O_2 (45 mL) at ice-bath under quickly stirring until obtaining a clear and transparent yellow solution. The obtained mixture was continued with stirring overnight for decomposing residual H_2O_2 and then peroxomolybdate (PM) was obtained after diluting the above mixture into 2 wt% solutions. Fig. S2b indicates the stability of PM through a powder X-ray diffraction pattern. To prepare PM/CNC composite film. 4 mL of CNC suspension after sonication for 10 min were firstly mixed with 2.0 mL of PM and stirred at room temperature for 1 h access to a homogeneous mixture. Briefly, the mixture was transferred into polystyrene Petri dishes (5 cm) to organize into a chiral nematic phase. During slow solvent evaporation for 48 h, the formation of iridescent yellow PM/CNC composite film with chiral nematic structure. Additional samples were prepared by using an identical procedure except for varying the amount of PM.

Preparation of chiral nematic mesoporous molybdenum carbide film. The as-prepared MCF-2.0 was first carbonized by heating the sample under flowing nitrogen to 600°C for 6 h to generate MoO_3/C composites. The black MoO_3/C materials (80 mg) and Mg turnings (400 mg) were placed at a ceramic reaction boat and annealed under flowing nitrogen to 650°C at a rate of 2°C min ^{1} and held at this temperature for 12 h.

Excess Mg was used to ensure the complete reduction of MoO_3. The resulting Mo_2C/C composites after magnesiothermic reduction were then calcined at 400°C in air for 1 h to eliminate residual carbon, giving chiral nematic mesoporous Mo_2C films before Mo_2C/C were treated with 0.5 M HCl at room temperature for 2 h to dissolve the MgO byproduct.

Electrochemical experiments. All the electrochemical experiments were conducted on an electrochemical workstation (CHI 760e). For the HER of two catalysts, a three-electrode cell was operated in 0.50 M H_2SO_4. Typically, 3 mg of catalyst and 80 mL of 5 wt% Nafion solution were dispersed in 1 mL of a solution of deionized water and ethanol (4:1 in volume ratio) [33]. After sonication for 30 min, 5 uL catalyst slurry was dropped onto smooth glassy carbon electrodes with a diameter of 3 mm and dried in an oven of 30°C. The mass loading was about 0.213 mg cm ^{2}. Carbon rod and Ag/AgCl (in 1.0 M KCl) were used as the counter and reference electrodes, respectively. The linear sweep voltammograms were collected in an H_2-purged cell at a scan rate of 5 mV s ^{1}. To estimate the electroactive surface area of Mo_2C, cyclic voltammograms were measured between 0.10 0.30 V vs. SHE with scan rates of 20, 50, 75, 100, 150, and 200 mV s ^{1}. Electrochemical impedance (EIS) measurements were carried out from 100 kHz to 0.1 Hz with an amplitude of 10 mV at selected values of overpotentials. The potential was converted to SHE via the equation: $E_{SHE} = E_{Ag/AgCl} + 0.059pH + E^{o}_{Ag/AgCl}$.

Results and discussion

A typical preparation of freestanding PM/CNC composite film is illustrated in Scheme 1. CNC suspension (4 wt%, pH =2.6) was mixed with a volume of yellow PM

(2 wt%, pH=1.9), subsequently obtaining a homogeneous PM/CNC mixture (Fig. S1a). Some small tactoids are observed through POM after the water evaporated for 12 hours (Fig. S1b). Then totally drying under ambient temperature, iridescent PM/CNC composite films were obtained (Fig. 1a). Thermogravimetric analysis (TGA, Fig. S2c) reveals the thermal decomposition of PM between 50 and 250°C, and PM has an overall mass loss of ~80 wt%. Infrared spectra (IR, Fig. S2d) of the PM solid shows a series of ~3640 cm^{1} ~1620 cm^{1}[34], Mo=O at ~980 and 940 cm^{1} ~630 cm^{1}[35, 36]. These features indicate that PM can form a stable self-assembled structure in the CNC aqueous solution.

Our approach to regulating the chiral nematic structure of PM/CNC films (MCFs) was operated by the modulation of PM loadings with a range of 1.0, 1.5, 2.0, and 2.5 mL. Fig. 1a shows three iridescent MCFs (i.e., MCF-1.0, MCF-1.5, and MCF-2.0 with a diameter of 5 cm), changing from blue, green to yellow in appearance. This color variation was recorded by UV-Vis spectroscopy (Fig. 1b upper panel), displaying as an obvious red-shift in transmission peaks. This color-changing was also observed in their POM images (Fig. 1c), along with a strong birefringence characteristic of chiral nematic ordering. CD spectra (Fig. 1b lower panel) show intense signal peaks with intensity greater than 2,000 millidegrees for all of the MCFs. This confirmation indicates the left-handed chiral nematic structure of these films. Besides, their CD shows a similar peak shift with that of the UV-vis. To the best of our knowledge, no attempt has yet been made to prepare the Mo-based composite films of intensely optical activity. These pieces of evidence demonstrate the MCF composite films can be endowed with the chiral nematic phase of CNC and the tunable chiral nematic structure was available through controlling the amount of PM. However, when the 2.5 mL volume of PM was added into CNC suspension, the casting MCF-2.5 (Fig. S3a) shows the weak character of the chiral nematic phase as confirmed by POM (Fig. S3b) and SEM (Fig. S3c).

Confirmed by the above investigation, these MCF composites show the tunability of the chiral nematic structure. This tunability can be explained by the following de Vries equation:[37] $\lambda_{max} = n_{avg} \cdot P$, where $_{\text{max}}$ is the reflected wavelength at normal incident light. n_{avg} and P are the average refractive index and helical pitch of the material, respectively. The reflected wavelength from MCF-1.0, MCF-1.5, to MCF-2.0 shows a red-shifted reflectance as recorded through UV-Vis spectra (Fig. 1b), which could explain through the increase of n_{avg} or P in these films. SEM recorded their actual P values that correspond to successive bilayer distances. The cross-sectional SEM images of these films show similar periodic layered structures but different in the increase of interlayer distances (Fig. 1d, 286, 381, and 550 nm). Furthermore, there is another attention in the SEM images of MCF-2.0 that rod-like morphology of obvious twisting in a counter-clockwise direction presents the left-handed chiral nematic structure. The resulting is consistent with the positive absorption band in CD. These investigations provide solid evidence that a self-assembly route to MCF is available, and their chiral structure easily realizes modulation through a ratio control of PM loading into the CNC system.

As proof of concept, CNC bio-templates can be used to make the large-area chiral molybdenum-based film. A versatile MCF-2.0 was firstly pyrolyzed under N_2 at 600^{o}C, giving a bulk glossy black MoO$_3$/C film (Fig. 2a). The cross-sectional SEM images of MoO$_3$/C film (Figs. 2b, c) show a similar successive layer to MCF-2.0 in Fig. 1d, except that the bilayer distance of MoO$_3$/C film is narrower. The conversion process of MCF-2.0 into MoO$_3$/C film was determined by TGA (Fig. 2d) and PXRD (Fig. 2e). The TGA curve of MCF-2.0 shows an approximate 35 % yield of carbon in MoO$_3$/C composite. MoO$_3$/C presents excellent thermal stability due to the formation of crystalline structures. The structural composition was confirmed by XRD patterns. MCF-2.0 shows two broad characteristic peaks of the CNC crystalline at 2 16° and 24°. After carbon conversion, MoO$_3$/C shows the disappeared characteristic peaks of CNC, and three new peaks appeared at 2 37°, and 52° that belonged to MoO$_3$ crystals[17, 38, 39]. These investigations confirm that the chiral nematic order of the CNC is reserved and the carbonization reaction converted the PM to MoO$_3$.

To prepare the porous Mo$_2$C film, the above MoO$_3$/C film was treated through magnesiothermic reduction, producing a colorful hybrid film (Fig. S4). Then, the treatment of the hybrid with an aqueous HCl solution removed residual MgO. Finally, an iridescent molybdenum carbide film (CN-Mo$_2$C, Fig. 3a) was obtained. CN-Mo$_2$C shows the strong birefringence in the POM image (Fig. 3b and Video S1). CN-Mo$_2$C presents a -phase, which PXRD pattern (Fig. 3e) demonstrates three typical characteristic peaks of (002), (110), and (101)[33]. It is recognized that the unique property of chiral nanostructure is the optical activity, in which this property is associated with the circular dichroism phenomenon[40, 41]. CD spectra of the CN-Mo$_2$C (Fig. 3f) show a broadband polarization absorption, while the C-Mo$_2$C (black

that the chiral nematic structure of CNC is embedded in the mesoporous Mo_2C, and this strategy can be used in other metal-based materials.

An important application for porous Mo_2C is in electrocatalytic HER production, which shows an excellent conductivity of $2.4\times10^{\ 2}$ S cm$^{\ 1}$ at 25°C. We evaluated the electrocatalytic activity of CN-Mo_2C and C-Mo_2C for HER by linear sweep voltammetry (LSV) in 0.50 M H_2SO_4[46, 47]. Fig. 4a shows the polarization curves with a scan rate of 5 mV s$^{\ 1}$. In this experiment, each catalyst with an approximately loading amount of 0.213 mg·cm$^{\ 2}$ was coated on glassy carbon. Furthermore, we used the Tafel slope to study the intrinsic activity of catalysts of hydrogen evolution, in which a smaller Tafel slope represents a faster HER efficiency[48]. According to the Tafel equation: $\ = b\log(j) + a$, where is the overpotential, b, j, and a are the Tafel slope, current density, and constant, respectively. Tafel analysis (Fig. 4b) gave two slopes of 88 and 148 mV·dec$^{\ 1}$ with relevant to CN-Mo_2C and C-Mo_2C, respectively. Molybdenum has attracted numerous research interests due to its Pt-like electronic structure. As a result, a series of sophisticated and extraordinary molybdenum-based catalysts have emerged, including molybdenum phosphide[49], $MoNi_4$[50], and molybdenum disulfide[51]. Compared with these reported systems, this CN-Mo_2C not only has a large-area and low-cost economy but also shows a well-recognized electrocatalytic activity. Evidentially, the chiral nematic nanostructure of CN-Mo_2C contributed to a higher exposed surface area, leading to higher specific current density and a smaller Tafel slope. The electroactive surface area of a catalyst is a critical factor for evaluating HER. Cyclic voltammetry (CV, Fig. 4c) of CN-Mo_2C was performed continuously in 0.5 M H_2SO_4 and recorded between 0.10 and 0.30 V versus reversible hydrogen electrode (RHE). The CV of CN-Mo_2C shows a rectangular shape with no noticeable redox peaks, indicating a

scan rates. Electrochemical impedance spectroscopy is another important criterion for studying the transport kinetics of electrocatalyst. Fig. 4d shows the Nyquist plot of CN-Mo_2C and C-Mo_2

that CN-Mo_2C has one smaller depressed semicircle in the high-frequency region resulting from its small charge transfer resistance. Demonstrating that the large BET surface area likely facilitated the high HER activity[52].

Conclusions

In summary, chiral nematic mesoporous Mo_2C films were first synthesized through the self-assembly of CNC with water-soluble PM. The Mo_2C film shows remarkable chiroptical properties and ordered helical layers via CD and SEM characteristics. This strategy can be extended to develop novel chiral Mo-based or Mo-derived materials with desirable functionalities. Following this study, numerous multi-type chiral inorganic materials (V_2C, TiC, or V-Mo binary hybrid) with a broadband chiroptical activity can be created.

Declaration of interests

Acknowledgements

This work was supported by the National Natural Science Foundation of China

(21775116 and 21922411), LiaoNing Revitalization Talents Program (XLYC1802109) and DICP Innovation Funding (DICP-RC201801).

References

[1] Z. Cheng, Y. Ma, L. Yang, F. Cheng, Z. Huang, A. Natan, H. Li, Y. Chen, D. Cao, Z. Huang, Y. Wang, Y. Liu, R. Yang, H. Zhu, Adv. Opt. Mater. 0 (2019) 1801816.

[2] L. Xu, M. Sun, P. Cheng, R. Gao, H. Wang, W. Ma, X. Shi, C. Xu, H. Kuang, Adv. Funct. Mater. 28 (2018) 1707237.

[3] T. Yutthalekha, C. Wattanakit, V. Lapeyre, S. Nokbin, C. Warakulwit, J. Limtrakul, A. Kuhn, Nat. Commun. 7 (2016) 12678.

[4] Y. Xia, Y. Zhou, Z. Tang, Nanoscale 3 (2011) 1374.

[5] W. Ma, L. Xu, A.F. de Moura, X. Wu, H. Kuang, C. Xu, N.A. Kotov, Chem. Rev. 117 (2017) 8041-8093.

[6] Y. Li, X. Wang, J. Miao, J. Li, X. Zhu, R. Chen, Z. Tang, R. Pan, T. He, J. Cheng, Adv. Mater. 32 (2020) 1905585.

[7] S. Che, Z. Liu, T. Ohsuna, K. Sakamoto, O. Terasaki, T. Tatsumi, Nature 429 (2004) 281-284.

[8] H.E. Lee, H.Y. Ahn, J. Mun, Y.Y. Lee, M. Kim, N.H. Cho, K. Chang, W.S. Kim, J. Rho, K.T. Nam, Nature 556 (2018) 360-365.

[9] Q. Jiang, X. Xu, P.-A. Yin, K. Ma, Y. Zhen, P. Duan, Q. Peng, W.-Q. Chen, B. Ding, J. Am. Chem. Soc. 141 (2019) 9490-9494.

[10] W. Jiang, Z.-b. Qu, P. Kumar, D. Vecchio, Y. Wang, Y. Ma, J.H. Bahng, K. Bernardino, W.R. Gomes, F.M. Colombari, A. Lozada-Blanco, M. Veksler, E. Marino,

A. Simon, C. Murray, S.R. Muniz, A.F. de Moura, N.A. Kotov, Science (2020) eaaz7949.

[22] K.R. Phillips, T. Shirman, E. Shirman, A.V. Shneidman, T.M. Kay, J. Aizenberg, Adv. Mater. 30 (2018) 1706329.

[23] A. Ivanova, B. Frka-Petesic, A. Paul, T. Wagner, A.N. Jumabekov, Y. Vilk, J. Weber, J. Schmedt auf der Günne, S. Vignolini, M. Tiemann, D. Fattakhova-Rohlfing, T. Bein, ACS Appl. Mater. Interfaces 12 (2020) 12639-12647.

[24] T. Hiratani, O. Kose, W.Y. Hamad, M.J. MacLachlan, Mater. Horiz. 5 (2018) 1076-1081.

[25] R.M. Parker, G. Guidetti, C.A. Williams, T. Zhao, A. Narkevicius, S. Vignolini, B. Frka-Petesic, Adv. Mater. 30 (2018) 1704477.

[26] W. Chen, H. Yu, S.-Y. Lee, T. Wei, J. Li, Z. Fan, Chem. Soc. Rev. 47 (2018) 2837-2872.

[27] M.H. Dickman, M.T. Pope, Chem. Rev. 94 (1994) 569-584.

[28] L. Zong, C. Wang, A.M.P. Moeljadi, X. Ye, R. Ganguly, Y. Li, H. Hirao, C.-H. Tan, Nat. Commun. 7 (2016) 13455.

[29] L. Liao, S. Wang, J. Xiao, X. Bian, Y. Zhang, M.D. Scanlon, X. Hu, Y. Tang, B. Liu, H.H. Girault, Energy Environ. Sci. 7 (2014) 387-392.

[30] T. Ouyang, A.-N. Chen, Z.-Z. He, Z.-Q. Liu, Y. Tong, Chem. Commun. 54 (2018) 9901-9904.

[31] F. Zhang, D. Wang, H. Qin, L. Feng, X. Liang, G. Qing, ACS Appl. Mater. Interfaces 11 (2019) 13114-13122.

[32] T. Abitbol, E. Kloser, D.G. Gray, Cellulose 20 (2013) 785-794.

[33] C. Tang, A. Sun, Y. Xu, Z. Wu, D. Wang, J. Power Sources 296 (2015) 18-22.

[34] T.-D. Nguyen, E. Lizundia, M. Niederberger, W.Y. Hamad, M.J. MacLachlan, Chem. Mater. 31 (2019) 2174-2181.

[46] H.B. Wu, B.Y. Xia, L. Yu, X.-Y. Yu, X.W. Lou, Nat. Commun. 6 (2015) 6512.

[47] H. Zhang, Z. Ma, G. Liu, L. Shi, J. Tang, H. Pang, K. Wu, T. Takei, J. Zhang, Y. Yamauchi, J. Ye, Npg Asia Mater. 8 (2016) e293.

[48] H. Wang, X. Xu, B. Ni, H. Li, W. Bian, X. Wang, Nanoscale 9 (2017) 15895-15900.

[49] X. Chen, D. Wang, Z. Wang, P. Zhou, Z. Wu, F. Jiang, Chem. Commun. 50 (2014) 11683-11685.

[50] J. Zhang, T. Wang, P. Liu, Z. Liao, S. Liu, X. Zhuang, M. Chen, E. Zschech, X. Feng, Nat. Commun. 8 (2017) 15437.

[51] J. Benson, M. Li, S. Wang, P. Wang, P. Papakonstantinou, ACS Appl. Mater. Interfaces 7 (2015) 14113-14122.

[52] G. Humagain, K. MacDougal, J. MacInnis, J.M. Lowe, R.H. Coridan, S. MacQuarrie, M. Dasog, Adv. Energy. Mater. 8 (2018) 1801461.

Scheme 1. Schematic illustrating of PM/CNC films with a chiral nematic structure owing to the self-ordering of CNC templates.

Fig. 1. Characterization data of three PM/CNC composite films. (a) Photographs of these films, from left to right: MCF-1.0, MCF-1.5, and MCF-2.0 (diameter, 5 cm) showing different structural colours under white light illumination. (b) UV-vis transmission spectra and positive CD spectra of PM/CNC films with the increasing amounts of PM loading showing a red-shift wavelength. (c) POM

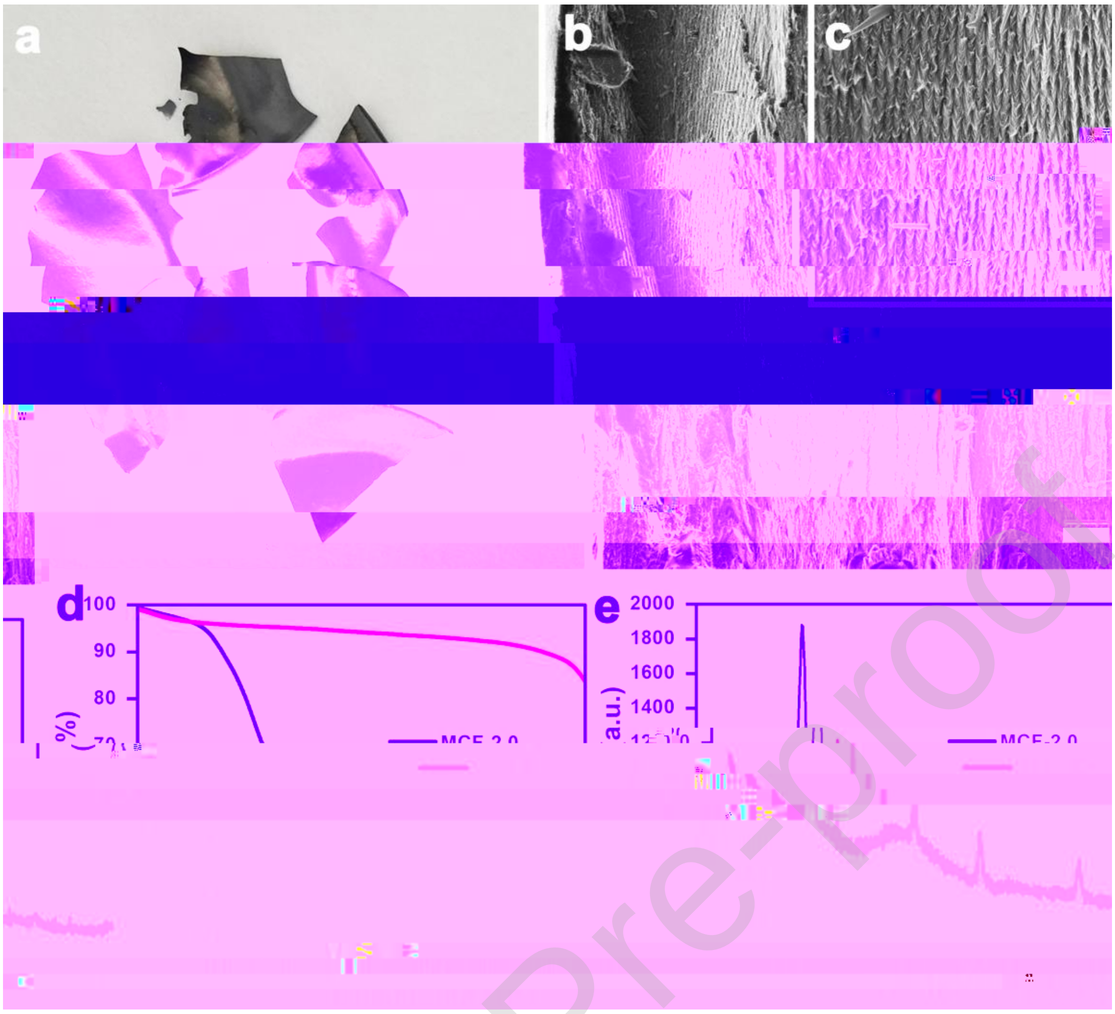

Fig. 2. Conversion of MCF-2.0 into MoO_3/C film. (a) Photos of MoO_3/C films with a bulk glossy black appearance (scale bar, 1 cm). (b) SEM images of fracture cross-section of MoO_3/C film shows the stacked layers of the chiral nematic phase (scale bar, 2 . (c) Higher magnification reveals the helical pitch distance (scale bar, 500 nm). TGA curves (d) and PXRD patterns (e) of the MoO_3/C composites after the carbonization of MCF-2.0.

Fig. 3. Freestanding CN-Mo_2C films prepared from MoO_3/C film. (a) Photos of iridescent CN-Mo_2C films (scale bar, 1 cm) and (b) POM image of CN-Mo_2C film (scale bar, 100 μm). (c, d) SEM images of the surface and fracture cross-section of CN-Mo_2C film (scale bar, 500 nm). (e) XRD patterns of CN-Mo_2C. (f) CD signal showing the CN-Mo_2C (red) of the positive absorption, and commercial Mo_2C (C-Mo_2C, black) no absorption band. (g) Nitrogen adsorption-desorption isotherms of CN-Mo_2C films and inset of a BJH pore size distribution.

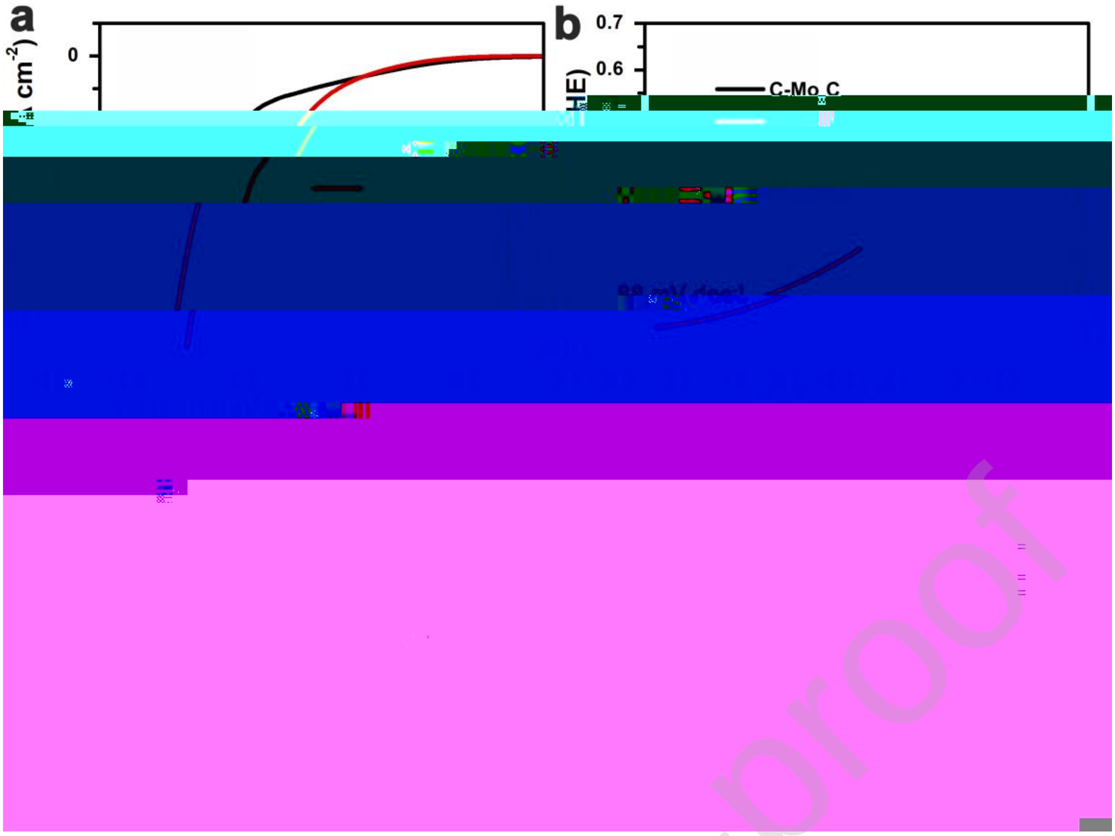

Fig. 4. (a) Polarization curves and (b) Tafel plots of CN-Mo_2C and commercial Mo_2C catalysts. (c) CVs curves of CN-Mo_2C at various scan rates between 20 and 200 mV s ^{1}. (d) Nyquist plots of CN-Mo_2C and commercial Mo_2C at an overpotential of 400 mV.